Local structure of indium in quinary (InGa)(AsSbN)/GaAs quantum wells

Jingli Chen,[1,2] Gianluca Ciatto,[1,3,*] Melanie Le Du,[2] Jean-Christophe Harmand,[2] and Frank Glas[2]
[1]*European Synchrotron Radiation Facility, BP 220, 38043 Grenoble Cedex 9, France*
[2]*Laboratoire de Photonique et Nanostructures, CNRS, Route de Nozay, 91460 Marcoussis, France*
[3]*Synchrotron SOLEIL, L'Orme des Merisiers, Saint-Aubin, BP 48, 91192 Gif-sur-Yvette Cedex, France*
(Received 10 May 2010; published 3 September 2010)

We performed In *K*-edge x-ray absorption fine-structure spectroscopy on (InGa)(AsSbN)/GaAs quinary quantum well samples exposed to annealing of different durations, in order to investigate their microstructures. Spectra neither evidence large modification as a function of annealing, nor are sensitive to In-N preferential ordering with the concentration at play. Nevertheless, we observed a shoulder on the low-*R* side of the Fourier-transformed spectra of all samples. This feature can be properly simulated under the hypothesis of formation of a complex where In atoms see a heavy nearest neighbor at a rather short distance. Mass and distance of the complex are compatible with a Sb-N split interstitial with the Sb atom located close to In. The concentration of this complex structure (roughly 2–3 % of the total In atoms) does not change substantially after the 800 °C annealing processes.

DOI: 10.1103/PhysRevB.82.125303 PACS number(s): 42.55.Px, 61.05.cj, 61.66.Dk, 81.05.Ea

I. INTRODUCTION

The group of (In,Ga)(As,N) materials has attracted considerable interest in the last 15 years due to their unusual electronic properties which make them suitable candidates for GaAs-based quantum-well (QW) lasers working in the wavelength of 1.3–1.55 μm. It was found that in different N composition range, the dilute alloys show different electronic properties. This is believed to be due to the different N neighborhood structures. The different microstructure of the alloy lead to different electronic structures of the material, and thus affect subsidently the optical properties and device performance.[1–5] In the study of fundamental properties, the change in microstructure of alloys in different N composition range makes the testification of the present theories interpreting the large band-gap lowing of this group of materials[6–11] rather difficult. Thus, a better understanding of the details of the N-induced microstructure is of great importance.

On the other hand, annealing processes are generally used to improve the quality of dilute nitride alloys; such annealing induces an unwanted blueshift of the band gap[12–16] and the alloy microstructure is believed to change during annealing.[17–20] Thus, the investigation on the structural effects of different annealing processes in dilute nitrides is also important.

X-ray absorption fine-structure spectroscopy (XAFS) has been already used in the study of the local structure of dilute nitride [$In_xGa_{1-x}As_{1-y}N_y$ (Refs. 21 and 22)], nitride-antimonide [$GaAs_{1-y-x}N_ySb_x$ (Ref. 23)] and, more recently, dilute bismide alloys [$GaAs_{1-y}Bi_y$ (Ref. 24)]. The same technique played an important role in solving simple defective structures in GaAs-based alloys, such as that of N-H complexes in $GaAs_{1-y}N_y$ (Ref. 25) and Mn-H complexes in $Ga_{1-x}Mn_xAs$.[26] In the present work, we used In *K*-edge XAFS to study the local structure around In atoms in quinary (InGa)(AsSbN) QWs, materials of particular importance for the manufactory of laser devices working near the second minimum of attenuation in optical fiber (1.55 μm),[27] and possible atomic-dimensional structural changes during thermal annealing with different durations.

II. EXPERIMENT

The samples were grown by solid-source molecular-beam epitaxy on semi-insulating GaAs (100) substrates.[27] The growth chamber was equipped with a radio-frequency plasma cell as the N source. Growth temperature for the quantum wells was 410 °C. The samples consist of multiquantum-well structures (3 repetitions) of thickness 8 nm separated by 15 nm of GaAs and covered by a GaAs cap 50 nm thick. Annealing was performed at 800 °C. The as-grown sample (QW0) and samples after annealing of 15 s (QW15) and 60 s (QW60) were studied in this work, photoluminescence (PL) measurements (not reported here) showed a blueshift of the emission peak of 135 nm for QW60 with respect to QW0. The concentration and annealing conditions of the three samples under study are reported in Table I.

TABLE I. Characteristics of the (InGa)(AsSbN) samples under study, including concentrations, annealing temperature, and duration.

Sample	In (%)	N (%)	Sb (%)	T_{anneal} (°C)	Time (s)
QW0	38	2	7.5	No	No
QW15	38	2	7.5	800	15
QW60	38	2	7.5	800	60

XAFS measurements were performed at the BM29 beam line of the European Synchrotron Radiation Facility (ESRF) using a two crystals Si (311) monochromator. Higher-order harmonics were rejected by exploiting two Pt-covered mirrors and detuning the monochromator crystals. The In *K*-edge absorption cross-section energy dependence was taken in the fluorescence mode with a 13-element Ge hyperpure detector. We measured the three QWs and InAs, InSb, and InN standard samples in the same experimental conditions for energy calibration and analysis purpose.

III. DATA ANALYSIS

A. Data treatment and analysis strategy

The XAFS oscillation extraction was executed by using the IFEFFIT package.[28] The E_0 was determined by the derivative minimum at the pre-edge and a cubic spline was used to interpolate the background. The $\chi(k)$ data were multiplied by a weighting function k^2, multiplied by a window and then Fourier transformed into real space.

In the simulation, a theoretical model was built by giving as input to the FEFF8 code[29] a trial structure. The theoretical signal was expressed as a sum over the paths of the photoelectron. Each term in this sum is the contribution to the XAFS signal by a component of the photoelectron that travels from the absorbing atom and then is scattered from one or more neighboring atoms and finally returns to the absorbing atom, following a specific path.[30] For each path there are several adjustable parameters optimized by IFEFFIT to fit the data. These parameters include the passive electron reduction factor (S_0^2), the number of identical paths (N_{degen}), the relative mean-square displacement [Debye-Waller (DW) factor] of the atoms included in path i (σ_i^2), an energy shift for each path (ΔE_{0i}), and a change in the path length in path i (Δr_i). Several of our models include as many as four paths, and therefore, several constraints were used to reduce the number (and correlation) of fit variables and maximize the degrees of freedom of the fit. These constraints are discussed in detail in the following: (a) S_0^2 N_{degen} and S_0^2 are both constant multiplication factors in the XAFS theory used to construct the models. Therefore, only the product $N_{degen}S_0^2$ can be determined. In *K*-edge data of a InAs standard sample was collected to decouple these constants. The crystallographic structure for InAs is known, so N_{degen} is no longer a fitted parameter. Thus the value for S_0^2 of 1.0428 ± 0.0283 was determined by the fitting of the XAFS data of the InAs standard sample taken in transmission mode.

(b) *Debye-Waller factor.* According to the correlated Debye and Einstein models of mean-square relative displacement,[31,32] DW factor of an absorber-backscatterer pair is reversed proportional to the effective mass of the two-atom system,

$$M = \frac{M_1 M_2}{M_1 + M_2}. \quad (1)$$

In Eq. (1), M_1, M_2 are the atomic mass of the two atoms, respectively while M is the effective mass of the two-atom system. In the fitting procedure, the DW factors for In-Sb, In-N bonds were set based on the DW factor of the In-As bond according to Eq. (1).

TABLE II. Paths and variables used to simulate In *K*-edge data (first shell analysis) with the four models used in this work.

Path	Atomic type	Δr	σ_i^2	Fraction
First	In→As	Δr_1	σ_1^2	$1-x-y$
Second	In→Sb	Δr_3	$\sigma_1^2 \times 0.767$	y
Third	In→N	Δr_2	$\sigma_1^2 \times 3.63$	x
Fourth	In→defect	Δr_4	$\sigma_1^2 \times$ ratio	z

When comparing two models, we used the reduced chi-square (RCS) as a measure of the goodness of fit, according to the definition of the FEFFIT code.[33] A decrease in the RCS value of one-sigma error ($\sqrt{2/k}$) (where k is the degrees of freedom of the fit) is regarded as the criterion of substantial improvement of the fit result. This determines when a parameter has to be treated as a variable itself or constrained to a function of the values of other variables.

B. (InGa)(AsSbN) samples and fit models

The experimental data were simulated by three different theoretical models. The three models contain two paths (In-As and In-Sb), three paths (In-As, In-Sb, and In-N), and four paths (In-As, In-Sb, In-N, and In defect), respectively. In each model, we used a common edge energy shift variable for all paths (ΔE_0). The DW factor of the In-As path was set as free of varying and the DW factor of other paths (In-Sb, In-N, and In defect) were set according to Eq. (1) as described above (variables used in the simulation are summarized in Table II).

The In-As bond length in the tetrahedral binary compounds (2.6233 Å),[34] which was tested by fitting the XAFS data of our standard sample, was given as a starting value for the length of the In-As path in the quinary samples, which was let free of varying in the simulation.

The spectra of all samples were first simulated with the model constructed with two paths: In-As and In-Sb. In each simulation, the amplitude of the In-As path was reduced by weighting with $(1-y)$ and the In-Sb path amplitude was increased by weighting with y to account for the contribution of Sb atoms to the backscattering of the first atomic shell. The In-Sb distance was varied within values less than the bond length of the binary compound [2.8057 Å (Ref. 35)] from 2.7063 to 2.8055 Å. The assumption of this construction of the trial structure is that in the main skeleton of the (InGa)(AsSbN) crystal, In-Sb atomic bond is expected to remain very close to the value it has in the corresponding binary compound, with a small reduction only.[36] The proportion of Sb atoms in the In neighborhood (y) was varied from 0.01 to 0.1. Varying both the In-Sb distances and Sb concentration y, we constructed a two-dimensional mesh with 70 trial structures. For each point of the mesh, we performed a fit with fixed bond length and concentration, testing the ability of each trial structure to reproduce the XAFS experimental data.

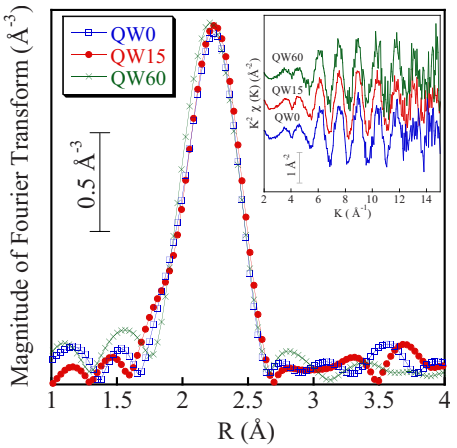

FIG. 1. (Color online) Fourier transform of the In *K*-edge XAFS data of samples QW15 (filled circle), QW0 (open square), and QW60 (cross). Inserted are the $k^2*\mathrm{chi}(k)$ spectra of the three samples.

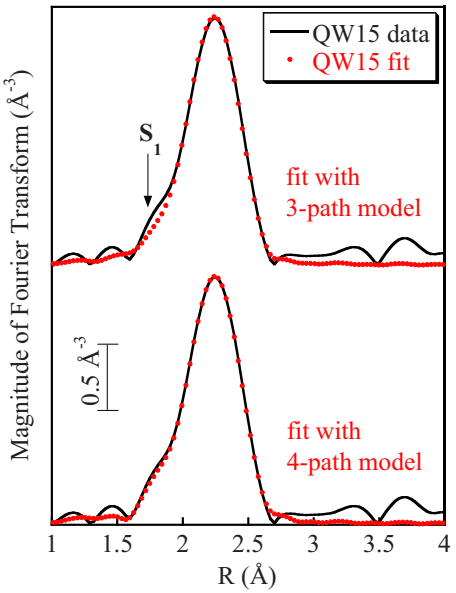

FIG. 2. (Color online) Fourier transform of the In *K*-edge data of sample QW15: experimental data (continuous line, top and bottom) and fits with a 3-path model (circles, top) and fits with a 4-path model (circles, bottom).

Subsequently, the spectra were simulated with trial structures composed of three paths: In-As, In-Sb, and In-N. In the simulation, the length of the In-Sb bond and the Sb fraction used in the fitting was the value with minimum RCS from the 2-path fitting. The In-N distance was varied around the bond length value in the binary InN alloy[37] (2.1356 Å) from 2.0785 to 2.3816 Å. The proportion of N atoms in the In neighborhood (x) was varied from 0.01 to 0.1.

Finally, we added a fourth path to mimic possible defective structures close to In atoms, as it will be detailed in Sec. IV. In the 4-path model, the relative In-Sb and In-N coordination numbers, and In-Sb and In-N bond lengths were fixed to the best fit values of the 3-path fitting.

IV. RESULTS

The In *K*-edge XAFS spectra from the three samples $[k^2*\mathrm{chi}(k)]$ and their Fourier transforms in R space are displayed in the inset and body of Fig. 1, respectively. The Fourier-transformed spectra show clearly the peak corresponding to the first coordination shell: the amplitude of such peak is similar for all samples, indicating that the number and type of In nearest neighbors should not change significantly upon annealing. Peaks corresponding to the second and third shells were not observable in the spectra, indicating that the local environment of In atoms is characterized by a high degree of structural disorder in the quantum wells. Negative interference between the In-In and In-Ga II shell paths gives an important contribution to the smoothing of the second shell peak. However, since second and third signals were not distinguishable from the noise, we focused on the analysis of the first shell only.

We first analyzed data from sample QW15 since its spectrum showed the highest signal to noise ratio among the three samples under study. The fitting range was 1.589–2.708 Å in R space and 4.247–14.936 Å^{-1} in K space. Using the 2-path model, the smallest numerical value for RCS was obtained with a Sb fraction of 2% and a In-Sb distance of 2.7410 Å: such values were fixed while fitting with the 3-path model, as anticipated in the previous section. After the fitting with the 2- and 3-path models with varying In-Sb and In-N distances and Sb, N concentrations y and x, we found the RCS resulting from these fits to lie close to each other. No one trial model is obviously better than the others. Upon fitting with In-Sb distances from 2.7063 to 2.8055 Å and Sb concentrations from 0 to 10%, the RCS values of 62 out of the 71 resulting models are within one-sigma error. The addition of an In-N path in the trial model resulted in increased RCS values, in the range of In-N distances of 2.0785–2.3816 Å and N atom concentrations of 0.5–10 %. This means that, with the concentration at play, we are not very sensitive to In-cation preferential binding, if existing. Only, we can exclude situations in which the relative In-Sb concentration number is higher than 7% and, at the same time, the In-Sb distance is either too close to the binary side (longer than 2.77 Å) or too short (smaller than 2.72 Å). This may give an indication that the relative In-Sb coordination number is smaller than the average nominal Sb concentration reported in Table I, but for central values of the bond length (2.74–2.75 Å) a In-Sb concentration=7.5% still lays within the one-sigma error bar of the lowest RCS. The result of the best fit obtained with the 3-path models is shown in Fig. 2 (top spectrum); actually, in case of sample QW15, this is a 2-path model fit being the In-N coordination set to zero due to the insensitivity to small In-N signals.

Looking at the figure, one can note that there is a shoulder on the low-R side of the first coordination shell peak (S_1) that cannot be reproduced with the structural models employed until now. In particular, although a similar feature observed in (InGa)(AsN) was previously attributed to preferential In-N binding,[21] we have showed here that it cannot be accounted for by simple addition of a In-N path. On the other hand, considering that our (InGa)(AsSbN) samples were grown under nonequilibrium conditions, it is likely that some amount

TABLE III. Minimum RCS values resulted with different defect masses in the 4-path simulation along with the corresponding In-defect distances and defect first shell fraction in the models (and the atoms used to mimic the defect).

Mass (a.u.)	28(Si)	73(Ge)	101(Ru)	108(Ag)	122(Sb)	133(Cs)	158(Gd)	209(Bi)
In-defect distance (Å)	2.08	2.08	2.04	2.04	2.04	2.04	2.04	2.04
First shell fraction	0.02	0.01	0.02	0.02	0.02	0.02	0.02	0.02
RCS	1.01	1.37	0.76	0.512	0.346	0.76	0.96	2.16

of structural defects is present within the samples. According to previous studies by other techniques on dilute nitrides, there are several kind of defects possibly existing in this kind of alloys.[3,19,38] Indeed, we made the hypothesis that the shoulder at the low-R side of the first shell peak (S_1) is due to a defective complex at a distance somewhat shorter than the average first shell distance.

In order to mimic the possible defect responsible for this feature in the spectra, we constructed models with a fourth path composed of atoms with different atomic masses and distances from the In atom, and tested their ability to reproduce the spectra. This was just an approximation to roughly identify the mass and the distance of the unknown defect. Table III lists the minimum RCS value obtained for each defect mass, the distance from In atoms and relative concentration of the defect, along with the name of the element used to mimic the defect (in brackets). The simulation showed a much reduced RCS value for atoms with mass of 122 ± 20 a.u. The minimum RCS value (0.346) was obtained for the mass of 122 a.u. (Sb). The RCS of this fit is sensibly lower than those of the models constructed with only 2 or 3 paths (Table IV). The simulation result obtained with this 4-path model is also shown in Fig. 2 (bottom spectrum). Improvement of the fit in the shoulder region is evident. This indicates that the S_1 related defect would have a mass close to 122 a.u., a In-defect distance of 2.035 Å, and concentration of about 2% of the total In atoms. Note that absolute values of the RCS extracted by FEFFIT (see software manual) do not have strict statistical sense, due to the poor estimation of the measurement uncertainty of the data and dependence on the Fourier transform parameters used, hence values smaller than 1 are perfectly possible for a good model and the basic rule when comparing two models is that the fit with the lowest RCS is the best.

In order to make sure that the low-R side shoulder (S_1) is not due to noise at the high k values which might induce errors in the background extraction, we changed the k-fitting range imposing a lower maximum k value of 12.091 $Å^{-1}$. In this simulation, the resulting change in RCS is in agreement with the fit result in the 4.247–14.936 $Å^{-1}$ k range. In fact, in the 4.247–12.091 $Å^{-1}$ k range, the fit with four paths resulted in an RCS value about 0.5 smaller than the one for the 3-path model. Figure 3 shows the best fitting results obtained with the 3- and 4-path models in the 4.247–12.328 $Å^{-1}$ k range. Despite the loss of resolution at low R due to the more drastic cutoff at high K, the fit with the 4-path model is still visually better than the others in the region of the shoulder.

We applied the same simulation procedures to the other two samples. The fitting range of the first coordination shell was 1.676–2.689 Å for QW0 and 1.751–2.692 Å for QW60. The fitting ranges in k space for QW0 and QW60 were 3.902–14.938 $Å^{-1}$ and 3.964–13.523 $Å^{-1}$, respectively. Similar results were obtained in the simulation of these two samples. Visually, the introduction of the fourth path always improves the fit. The RCS values obtained for the three samples using the different fitting models are listed in Table IV. In the simulation of sample QW0 data using the 2-path model, RCS values for 64 out of the 71 models were within one-sigma error, while using the 3-path model, 42 out of 55 mesh points were within one-sigma error. The fit with the 4-path model resulted in a RCS value (0.72) 1.51 lower than the best fit for the models with 2 and 3 paths (Table IV). The best fits obtained with the 3- and 4-path models on sample QW0 are shown in Fig. 4.

Finally, for sample QW60, in the 2-path approach 53 out of 71 RCS values were within one-sigma error; in the 3-path approach, 68 out of 78 RCS values were within the same error bar. The best fitting results obtained for sample QW60 with the 3- and 4-path model are displayed in Fig. 5. The fit with the 4-path model resulted a RCS value (0.336) 2.23 lower than the one of the best fit obtained with the 3-path model (Table IV).

V. DISCUSSION

There are several types of defects possibly present in the (InGa)(AsSbN) alloy. These include the N-N dimer, N-As,

TABLE IV. Best fit values for the path length (unit in Å) and the relative In-anion coordination number obtained with the 3- (or 2) and 4-path models, along with the RCS obtained with each model.

	With 2- and 3-paths model		With 4-paths model	
Sample No.	Best model	RCS	Best model	RCS
QW0	3 paths		In defect	
	In-Sb 2.728 2%	2.23	2.078 4%	0.725
	In-N 2.252 2%			
	In-As 2.576 96%			
QW15	3 paths		In-defect	
	In-Sb 2.741 2%	0.82	2.035 2%	0.346
	In-N 0%			
	In-As 2.582 98%			
QW60	3 paths		In-defect	
	In-Sb 2.641 5%	2.58	2.165 4%	0.336
	In-N 1.992 3%			
	In-As 2.581 92%			

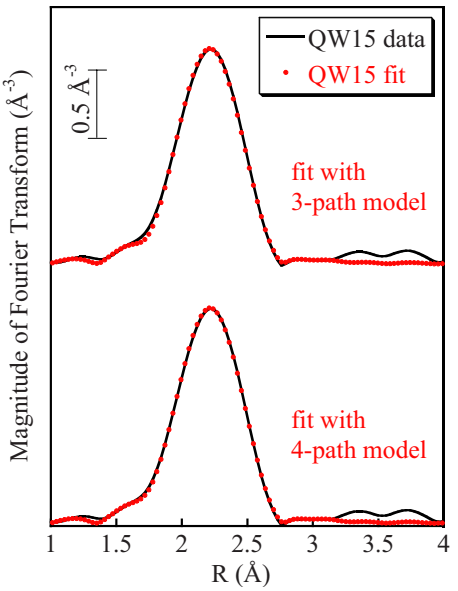

FIG. 3. (Color online) Fourier transform of the In K-edge XAFS spectrum of sample QW15, performed on a k range of 4.247–12.091 Å^{-1}: experimental data (continuous line, top and bottom) and fits with a 3-path model (circles, top) and with a 4-path model (circles, bottom).

and N-Sb interstitial pairs.[19,21,39–41] If the defect was a N-N dimer, both its average distance to the closest In atom and mass would be far from the values we extracted from our fits. Therefore we can exclude this possibility. We calculated also the distance between the As and In atoms, Sb and In atoms for the case of As-N or Sb-N interstitial pairs. We used the same method as Chen *et al.*[42] to introduce the interstitial pair of Sb-N and As-N in the (InGa)(AsSbN) crystal: in the (InGa)(AsSbN) alloy, the In atoms possess the group-III atoms' positions and, if we put the middle point of the Sb-N/As-N bond at the center of the tetrahedral composed with III-group atoms (as shown in Fig. 6), the distance between the Sb atom and its nearest In atoms is 2.091 Å in the case of a Sb-N pair, while the distance between the As and its closest In atom would be 2.113 Å in the case of a As-N pair. The average lattice constant of the (InGa)(AsSbN) alloy in Fig. 6 was approximated according to Vegard's law based on the lattice constants of GaAs and InAs as

$$a_{\mathrm{InGaAs}} = 0.62a_{\mathrm{GaAs}} + 0.38a_{\mathrm{InAs}}, \tag{2}$$

this approximation neglect N and Sb atoms (which effects, in any case, compensate) in the determination of the average lattice parameter, relying on their low concentration. The effective bond length between the Sb/As and N atoms is calculated as

$$d_{\mathrm{SbN}} = (r_{\mathrm{Sb}} + r_{\mathrm{N}})/2 \tag{3}$$

or

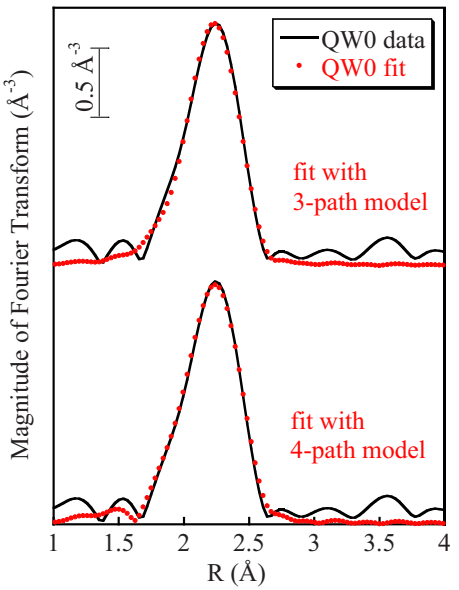

FIG. 4. (Color online) Fourier transform of the In K-edge data of sample QW0: experimental data (continuous line, top and bottom) and fits with the 3-path model (circles, top) and the 4-path model (circles, bottom).

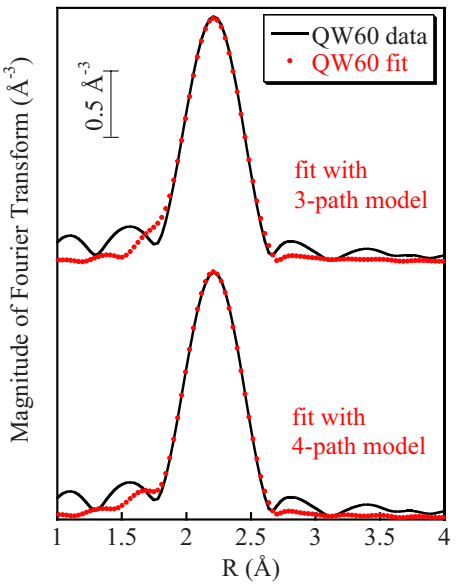

FIG. 5. (Color online) Fourier transform of the In K-edge data of sample QW60: experimental data (continuous line, top and bottom) and fits with the 3-path model (circles, top) and with the 4-path model (circles, bottom).

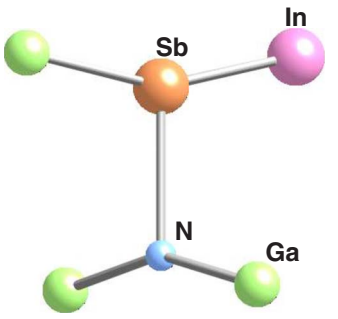

FIG. 6. (Color online) Configuration of Sb-N interstitial pair in the (InGa)(AsSbN) alloy.

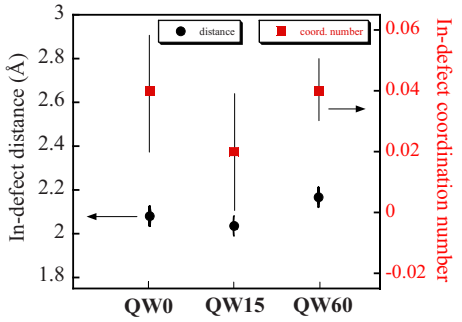

FIG. 7. (Color online) The In-defect distance and the defect fraction in the In-first shell extracted by fitting the data for samples QW0, QW15, and QW60.

$$d_{AsN} = (r_{As} + r_N)/2 \tag{4}$$

where r_{Sb}, r_{As}, and r_N are the covalent radii of Sb, As, and N atoms.

Even if our model of the defect is simplified (we have not calculated the relaxed atoms position via density-functional theory), we observe that in the hypothesis of formation of Sb-N split interstitials with the Sb atom close to an In one (such as in Fig. 6) the In atom would see a Sb atom (which mass is =122 a.u.) at a distance similar to the one which minimizes the RCS in our 4-path model (Table IV). At the same time, the XAFS signal from such In atom would be less affected by the presence of the N atom in the pair since N is a light backscatterer and is located further from the In atom with respect to Sb. Indeed, the component to the In *K*-edge XAFS signal due to backscattering from the Sb-N defective complex would be very similar to the one of the model structure (a single Sb atom) which permitted us to very well simulate the experimental XAFS in the 4-path approach. The fraction of defective complexes in the In first shell extracted from the fit (Table IV) is in the range 2–4 %. This may also justify the fact that the relative In-Sb coordination number (we mean here of the Sb atoms in As-substitutional position only, at about 2.7 Å) seems to be smaller than the average nominal Sb concentration, as suggested by the RCS analysis reported in Sec. IV: as a matter of fact, part of the Sb atoms move out from their substitutional position to be involved in the formation of Sb-N split interstitial defects.

Based on these considerations we propose that Sb-N split interstitials are present in all samples and are at the origin, at least in the case of (InGa)(AsSbN), of the low-*R* shoulder observed in the XAFS Fourier transform. Last step of the analysis was trying to monitor the change in the complex concentration and structure upon annealing. The simulations performed with the 4-path model revealed that the fraction of complexes remains at the same level, within one-sigma error bar, in the as grown sample and after annealing, as shown in Fig. 7 where we plot the defect concentration and the In-defect distance (in our picture, the Sb atom in the split interstitial) as a function of annealing. This confirms the first impression of the visual inspection of the Fourier-transform amplitudes (Sec. IV). However, with the uncertainties at play, we can neither claim nor exclude that partial defect annihilation or other process, including partial reaction,[21,39,40] occur during annealing. Finally, N-related defects seem to play minor or no role in the large blueshift of the band gap observed by PL upon annealing.

Therefore, the origin of the annealing-induced large band-gap blueshift observed in (InGa)(AsSbN) alloys remains still an open question. Due to the low sensitivity to In-N preferential binding related to the low N/In concentration ratio in our samples (in maximum ordering conditions In atoms would see only 5.3% N atoms as nearest neighbors), we cannot exclude the presence of weak short-range ordering similar to the one observed in InGaAsN:[22] this would give a contribution to the blueshift. In parallel, mechanisms related to the anion sublattice only, such as the breaking/modifications of N pairs proposed for quaternary GaAsSbN (Ref. 23) and annealing-driven homogenization of fluctuation in N concentration at a nanometric scale[16] can also contribute to the blueshift. The coexistence of different microstructural mechanisms may explain the larger blueshift observed in (InGa)(AsSbN) (75 meV) with respect to GaAsSbN (37 meV) and InGaAsN (27 meV) for similar annealing conditions. An investigation of the N local environment by N *K*-edge x-ray absorption near-edge structure spectroscopy would help in addressing the N-neighbor structure in these quinary quantum wells, however such experiment would be much more challenging with respect to our previous ones because of the lower thickness of the samples and the presence of a cap layer, in addition to the N dilution: in these conditions nitrogen surface contamination becomes an issue and the experiment would probably require UHV transfer from the MBE growth station.

VI. CONCLUSION

In summary, we performed In *K*-edge XAFS on (InGa)(AsSbN) quinary quantum wells, both in the as grown state and annealed under different durations. In the low-*R* side of the Fourier-transform first shell peak, we observed a shoulder that could only be simulated under the hypothesis of formation of a small fraction of defective complexes. Such defects are characterized by a large atomic mass at a small distance from In atoms. Based on the model which gives the best simulation of the experimental data, we suggest that the complex structure is a Sb-N split interstitial, where the Sb atom is located close to an In one. The concentration of such complexes does not significantly evolve after an annealing at 800 °C for 60 s, indeed they do not seem to play a role in the annealing-induced band-gap blueshift observed in these samples.

*Corresponding author; gianluca.ciatto@synchrotron-soleil.fr

[1] S. Francoeur, J. F. Klem, and A. Mascarenhas, Phys. Rev. Lett. **93**, 067403 (2004).
[2] G. Bentoumi, V. Timoshevskii, N. Madini, M. Côté, R. Leonelli, J.-N. Beaudry, P. Desjardins, and R. A. Masut, Phys. Rev. B **70**, 035315 (2004).
[3] Y. Zhang, A. Mascarenhas, J. F. Geisz, H. P. Xin, and C. W. Tu, Phys. Rev. B **63**, 085205 (2001).
[4] D. Karaiskaj, A. Mascarenhas, M. Adamcyk, E. C. Young, and T. Tiedje, Phys. Rev. B **74**, 035208 (2006).
[5] A. Patanè, J. Endicott, J. Ibáñez, P. N. Brunkov, L. Eaves, S. B. Healy, A. Lindsay, E. P. O'Reilly, and M. Hopkinson, Phys. Rev. B **71**, 195307 (2005).
[6] S. H. Wei and A. Zunger, Phys. Rev. Lett. **76**, 664 (1996).
[7] L. Bellaiche, S. H. Wei, and A. Zunger, Appl. Phys. Lett. **70**, 3558 (1997).
[8] L. Bellaiche, S. H. Wei, and A. Zunger, Phys. Rev. B **54**, 17568 (1996).
[9] L. Bellaiche, S. H. Wei, and A. Zunger, Phys. Rev. B **56**, 10233 (1997).
[10] W. Shan, W. Walukiewicz, J. W. Ager, E. E. Haller, J. F. Geisz, D. J. Friedman, J. M. Olson, and S. R. Kurtz, Phys. Rev. Lett. **82**, 1221 (1999).
[11] W. Shan, W. Walukiewicz, I. J. W. Ager, E. E. Haller, J. F. Geisz, D. J. Friedman, J. M. Olson, and S. R. Kurtz, J. Appl. Phys. **86**, 2349 (1999).
[12] T. Kageyama, T. Miyamoto, S. Makino, F. Koyama, and K. Iga, Jpn. J. Appl. Phys., Part 2 **38**, L298 (1999).
[13] I. A. Buyanova, G. Pozina, P. N. Hai, N. Q. Thinh, J. P. Bergman, and W. M. Chen, Appl. Phys. Lett. **77**, 2325 (2000).
[14] H. P. Xin, K. L. Kavanagh, Z. Q. Zhu, and C. W. Tu, Appl. Phys. Lett. **74**, 2337 (1999).
[15] L. H. Li, Z. Pan, W. Zhang, Y. W. Lin, Z. Q. Zhou, and R. H. Wu, J. Appl. Phys. **87**, 245 (2000).
[16] L. Grenouillet, C. Bru-Chevallier, G. Guillot, P. Gilet, P. Ballet, P. Duvaut, G. Rolland, and A. Million, J. Appl. Phys. **91**, 5902 (2002).
[17] E. V. K. Rao, A. Ougazzaden, Y. L. Bellego, and M. Juhel, Appl. Phys. Lett. **72**, 1409 (1998).
[18] Q. Gao, H. H. Tan, C. Jagadish, and P. N. K. Deenapanray, Jpn. J. Appl. Phys., Part 1 **42**, 6827 (2003).
[19] M. Ramsteiner, D. S. Jiang, J. S. Harris, and K. H. Ploog, Appl. Phys. Lett. **84**, 1859 (2004).
[20] N. Q. Thinh, I. A. Buyanova, W. M. Chena, H. P. Xin, and C. W. Tu, Appl. Phys. Lett. **79**, 3089 (2001).
[21] V. Lordi, V. Gambin, S. Friedrich, T. Funk, T. Takizawa, K. Uno, and J. S. Harris, Phys. Rev. Lett. **90**, 145505 (2003).
[22] G. Ciatto *et al.*, Phys. Rev. B **68**, 161201(R) (2003).
[23] G. Ciatto, J.-C. Harmand, F. Glas, L. Largeau, M. Le Du, F. Boscherini, M. Malvestuto, L. Floreano, P. Glatzel, and R. Alonso Mori, Phys. Rev. B **75**, 245212 (2007).
[24] G. Ciatto, E. C. Young, F. Glas, J. Chen, R. Alonso Mori, and T. Tiedje, Phys. Rev. B **78**, 035325 (2008).
[25] G. Ciatto *et al.*, Phys. Rev. B **79**, 165205 (2009).
[26] C. Bihler *et al.*, Phys. Rev. B **78**, 235208 (2008).
[27] L. H. Li, V. Sallet, G. Patriarche, L. Largeau, S. Bouchoule, L. Travers, and J. C. Harmand, Appl. Phys. Lett. **83**, 1298 (2003).
[28] M. Newville, J. Synchrotron Radiat. **8**, 322 (2001).
[29] A. L. Ankudinov, B. Ravel, J. J. Rehr, and S. D. Conradson, Phys. Rev. B **58**, 7565 (1998).
[30] P. A. Lee, P. H. Citrin, P. Eisenberger, and B. M. Kincaid, Rev. Mod. Phys. **53**, 769 (1981).
[31] G. Beni and P. M. Platzman, Phys. Rev. B **14**, 1514 (1976).
[32] E. Sevillano, H. Meuth, and J. J. Rehr, Phys. Rev. B **20**, 4908 (1979).
[33] M. Newville, B. Ravel, D. Haskel, J. J. Rehr, E. A. Stern, and Y. Yacoby, Physica B **208**, 154 (1995).
[34] G. Ozolins, G. Averkieva, A. Ievins, and N. Goryunova, Kristallografiya **7**, 850 (1962).
[35] S. Massidda, A. Continenza, A. J. Freeman, T. M. de Pascale, F. Meloni, and M. Serra, Phys. Rev. B **41**, 12079 (1990).
[36] J. C. Mikkelsen and J. B. Boyce, Phys. Rev. Lett. **49**, 1412 (1982).
[37] A. F. Wright and J. S. Nelson, Phys. Rev. B **51**, 7866 (1995).
[38] P. Krispin, V. Gambin, J. S. Harris, and K. H. Ploog, J. Appl. Phys. **93**, 6095 (2003).
[39] S. Dhar, N. Halder, A. Mondal, B. Bansal, and B. M. Arora, Semicond. Sci. Technol. **20**, 1168 (2005).
[40] A. Khan, S. R. Kurtz, S. Prasad, S. W. Johnston, and J. Gou, Appl. Phys. Lett. **90**, 243509 (2007).
[41] P. Carrier, S. Wei, S. Zhang, and S. Kurtz, Phys. Rev. B **71**, 165212 (2005).
[42] N. F. Chen, Y. Wang, H. He, and L. Lin, Phys. Rev. B **54**, 8516 (1996).